Organic Electronics 13 (2012) 58–65

Contents lists available at SciVerse ScienceDirect

Organic Electronics

journal homepage: www.elsevier.com/locate/orgel

Structural phase transition in pentacene caused by molecular doping and its effect on charge carrier mobility

Hans Kleemann *, Christoph Schuenemann, Alexander A. Zakhidov, Moritz Riede, Björn Lüssem, Karl Leo

Institut für Angewandte Photophysik, Technische Universität Dresden, George-Bähr-Straße 1, 01069 Dresden, Germany

ARTICLE INFO

Article history:
Received 11 August 2011
Received in revised form 22 September 2011
Accepted 29 September 2011
Available online 18 October 2011

Keywords:
Organic semiconductors
Molecular doping
Polycrystalline organic semiconductors
Doping induced structural transition
Charge carrier transport

ABSTRACT

The structural properties and charge carrier mobility of pentacene doped by 2,3,5,6-tetrafluoro-7,7,8,8-tetracyanoquinodimethane (F4-TCNQ) and 2,2-(perfluoronaphthalene-2,6-diylidene) dimalononitrile (F6-TCNNQ) are studied by X-ray diffraction, scanning electron microscopy, field effect transistor measurements, and space charge limited currents (SCLC). We observe the presence of polycrystalline and amorphous domains within the doped pentacene film grown under co-deposition conditions. The appearance of the amorphous phase is induced by the molecular dopants F4-TCNQ and F6-TCNNQ. A strong drop of crystallite size is obtained at a doping concentration of around 7 and 4 wt.%, respectively. The loss of the polycrystalline structure is correlated to a strong decrease of the charge carrier mobility in pentacene in horizontal and vertical film structures. We discuss typical scenarios of charge transport for polycrystalline and amorphous thin films in order to explain the observed loss of mobility originated by the doping induced structural phase transition. In this way an optimum doping concentration for highest conductivity with acceptable mobility is determined which can help to improve the performance of organic solar cells and organic high-frequency rectification diodes.

1. Introduction

Amorphous and polycrystalline organic semiconductors have received growing interest in recent years because of their promising properties for applications in the field of optoelectronics [1,2] and low-cost electronics [3–5]. Conductivities of organic semiconductors are usually rather low. A suitable way to overcome these conductivity restrictions is the concept of doping of organic semiconductors, which has been investigated extensively in theory [6] and experiment [7]. Although so far only a number of chemical compounds for dopants have been investigated, it is obvious that the design freedom of organic chemistry will offer many more materials, which together with the many possible organic semiconductors offer a wide freedom in stack design and device optimization with respect to the targeted application.

Several approaches for efficient doping have been found for organic semiconductors. A generation of mobile charge carriers by exposing the organic layer to strongly oxidizing gases [8], vapors of perfluorinated alkyl silanes [9], or by adding metal ions like lithium [10] has been shown. However, the doping of organic semiconductors by coevaporation of molecular dopants is usually more favorable in terms of stability and reproducibility [7]. For the well-known effective *p*-type dopant, 2,3,5,6-tetrafluoro-7,7,8,8-tetracyanoquinodimethane (F4-TCNQ), the principle of doping was investigated for materials like zinc-phthalocyanine (ZnPc) [11], *N*′,*N*′-tetrakis(4-methoxyphenyl)-benzidine (MeO-TPD) [12,13], *N*,*N*^{I}-diphenyl-*N*,*N*^{I}-bis(1-naphthyl)-1,10-biphenyl–4,4^{II}-diamine (NPB) [14] and pentacene [15]. For ZnPc [11] an increase and for pentacene [16]

* Corresponding author.
E-mail address: hans.kleemann@iapp.de (H. Kleemann).
URL: http://www.iapp.de (H. Kleemann).

1566-1199/$ - see front matter © 2011 Elsevier B.V. All rights reserved.
doi:10.1016/j.orgel.2011.09.027

a decrease in mobility was found without clarification of the corresponding effect in its entirety. A loss in conductivity for high doping concentrations was also reported by Brinkmann et al. [17] for iodine-doped pentacene.

In this contribution, we study the structural properties of pentacene films doped by F4-TCNQ, which is of interest for applications in organic thin film transistors (OTFT) [18], organic solar cells [19] and rectification diodes [3,20]. A structural phase transition in polycrystalline pentacene films induced by co-evaporation of F4-TCNQ is observed by X-ray diffraction (XRD) and scanning electron microscopy (SEM) investigations. Besides the structural modifications, we reveal a significant change in the electrical behavior. In particular, we determine a continuous decrease of charge carrier mobility, which is related to the loss of crystallinity. The reduced mobility is found for organic thin film transistors (OTFT) as well as for sandwiched films applicable for solar cells or rectification diodes. For comparison, we also investigate the doping of pentacene by the dopant 2,2-(perfluoronaphthalene-2,6-diylidene) dimalononitrile (F6-TCNNQ). The chemical structures of the molecules uses in this work are drawn in Fig. 1.

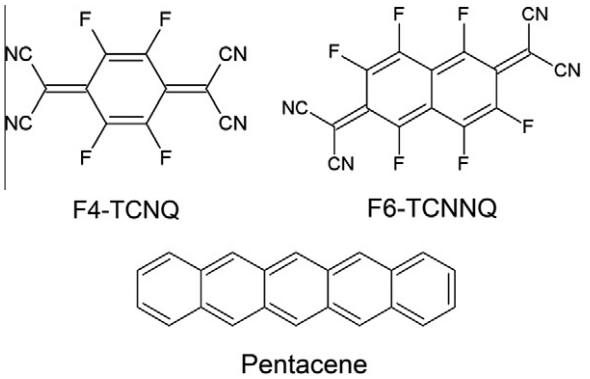

Fig. 1. Chemical structure of the dopants molecules F4-TCNQ and F6-TCNQ as well as the matrix material pentacene.

2. Experimental details

All films of pentacene doped by F4-TCNQ and F6-TCNNQ are fabricated by thermal co-evaporation of the materials under ultra high vacuum condition at a pressure of 10^{-5} Pa. Pentacene is evaporated at 190 °C and at a rate of 0.1 nm/s, while the temperature of the F4-TCNQ source is varied from 82 to 96 °C depending on the required doping concentrations (95 to 110 °C for F6-TCNNQ). The rates are checked during deposition by independent quartz crystal monitors for each material and the substrate temperature is kept at room temperature. Pentacene is purchased from Sensient, F4-TCNQ from abcr GmbH and F6-TCNNQ from Novaled AG Dresden. For the X-ray investigations, the organic films with an overall thickness of 150 nm are deposited onto naturally oxidized single crystalline (001) silicon substrates, which are pre-heated in a nitrogen glovebox for 1 h at 110 °C to remove remaining water from the surface. The XRD patterns are recorded in symmetric θ-2θ-scan by the X-ray powder diffractometer URD-6 (Seifert FPM, Germany) designed in Bragg–Brentano geometry using Cu-K_α radiation monochromatized by a secondary graphite monochromator and recorded by a scintillation detector under ambient conditions. During the measurements, the sample is rotated to minimize the influence of texture effect. The software PowderCell [21,22] is used to identify the crystallographic phase of pentacene. The crystallite size is determined with the software Analyze [23] and SIZECR [24] using the Cauchy–Cauchy-model (Williamson–Hall plot) [25]. The full procedure of the determination of crystallite size and microscopic strain is explained in reference [26].

A highly doped silicon wafer is used for the OTFT samples, which acts as the gate contact, with a 50 nm thick layer of Al_2O_3 as dielectric material produced by atomic layer deposition (ALD) (Oxford Instruments FlexAL). Substrates are pre-treated in the following sequence: acetone, ethanol, isopropanol for 5 min in an ultrasonic bath, boiling hexamethyldisilazan (HMDS) for 5 min, and finally spin rising by isopropanol. Afterwards, the organic layers are evaporated as described above and finally covered by source and drain electrodes consisting of 30 nm of gold patterned by a shadow mask. OTFT structures considered here have a channel length of 100, 50, and 30 μm and a channel width of 1000, 500, and 300 μm, respectively. The electrical investigations of the OTFT are done at room temperature in a nitrogen glovebox using two Keithley 2400 source measuring units. The mobility is determined in the saturation region of the OTFT performance.

The vertical device structures are manufactured on a cleaned glass substrate. For pentacene Schottky-diodes, we coat a 50 nm thick layer of Poly(3,4-ethylenedioxythiophene):poly(styrene sulfonate) (PEDOT:PSS) (CLEVIOS™ PH 1000, 6 vol.% ethylene glycol, conductivity of 700 S/cm) on an evaporated gold bottom contact (30 nm). Pedot:PSS is structured as described in [27] down to the size of the gold bottom contacts. Afterwards pentacene films (50, 100 and 150 nm to verify any thickness dependence) are prepared by thermal deposition as mentioned above. The stack is finished by an aluminum (Al) top contact (thickness 50 nm, rate 0.3 nm/s). Pentacene/Al is known to act as a good Schottky-contact [3]. The active area for Pentacene/Al Schottky-diodes is 0.01 mm^2. The current voltage (*IV*) characteristics of these samples are investigated by a Keithley 2400 source measuring unit.

3. Results and discussion

3.1. X-ray diffraction and electron microscopy studies

For the identification of the crystalline structure, the doped and undoped pentacene films are characterized by XRD. 150 nm thick films are employed to achieve sufficient scattering volume for detection of small crystallites. The observed XRD pattern scans for undoped pentacene and F4-TCNQ (4 and 8 wt.%) doped pentacene layers are shown in Fig. 2a. The XRD scans for the 2, 4, and 10 wt.% F6-TCNNQ doped pentacene films are shown in Fig. 2b. The undoped and all doped pentacene films which are crystalline consist

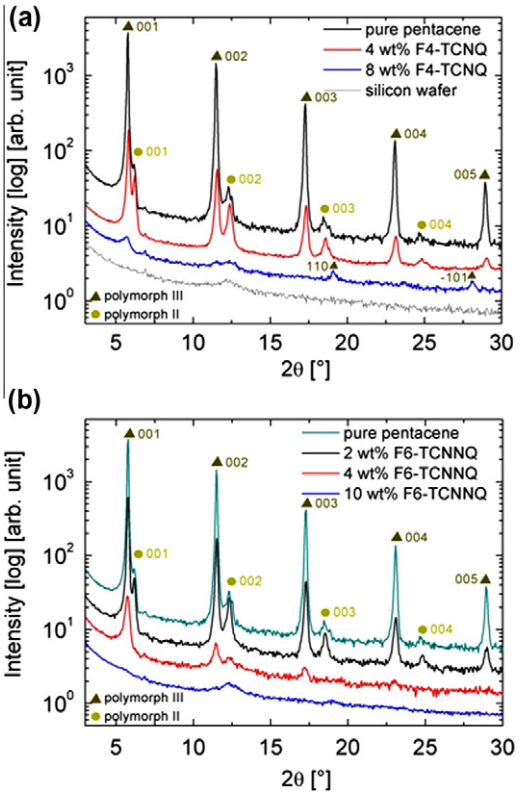

Fig. 2. XRD θ–2θ-scans of the undoped 150 nm thick pentacene film, the F6-TCNNQ doped pentacene film (a) and the F4-TCNQ doped pentacene film (b) at different molar doping concentrations. The XRD pattern of the silicon substrate used for the film deposition is shown in bottom of (b). The theoretical $2\theta_{Bragg}$ angle positions of the XRD reflections of the polymorph III [28] and polymorph II [29] pentacene modifications are indicated by different symbols together with *hkl* Miller indices.

Table 1
$2\theta_{Bragg}$ positions of the XRD reflections observed and calculated for polymorph III and the polymorph II phase of the undoped 150 nm thick pentacene film deposited on a silicon substrate. Miller indices *hkl* of corresponding reflections are indicated. Literature values for comparison are taken from [28,29].

Literature			
$2\theta_{Bragg}$ [°]	$2\theta_{Bragg}$ [°]	Reflection	Polymorph
5.76	5.74	001	III
11.49	11.48	002	III
17.25	17.26	003	III
23.07	23.08	004	III
28.94	28.97	005	III
6.15	6.19	001	II
12.29	12.40	002	II
18.45	18.64	003	II
24.67	24.94	004	II

Table 2
Crystallite sizes of the polymorph II and III phase of pentacene for different molar doping concentrations of F4-TCNQ and F6-TCNNQ. For the crystallite size values marked with * the determination of the error is not possible because only one Bragg reflection was obtained for each molecular orientation.

	Crystallite size [nm]	Polymorph	Bragg-reflection
Undoped	145 ± 27	III	001
	54 ± 37	II	001
2 wt.% F6-TCNNQ	71 ± 22	III	001
	42 ± 17	II	001
4 wt.% F6-TCNNQ	28 ± 5	III	001
		II	
4 wt.% F4-TCNQ	56 ± 13	III	001
	60 ± 33	II	001
8 wt.% F4-TCNQ	19	III	001
	23	III	110
	28	III	−101

of two triclinic phases which are well known from literature: the polymorph III (space group P-1, a = 5.958 Å, b = 7.596 Å, c = 15.6096 Å, α = 81.25°, β = 86.56°, γ = 89.8°) described by Schiefer et al. [28] and the polymorph II phase (space group P-1, a = 6.2749 Å, b = 7.8882 Å, c = 14.7095 Å, α = 76.014°, β = 87.233°, γ = 84.996°) found by Siegrist et al. [29]. In Table 1 the good agreement between observed Bragg reflections and the polymorph II and/or polymorph III phase is shown. For the pure pentacene films, we can only observe 001 reflections of both phases. This means that all pentacene molecules which are present in a crystalline phase are oriented in the same way. Due to the fact that all detected Bragg reflections result from the pentacene, we can exclude a crystallization of the dopant even at high doping concentrations of 20 wt.% F6-TCNNQ. A strong decrease of crystallinity is shown for both *p*-dopants starting at low doping concentrations of 2 wt.% F6-TCNNQ. This is evident from the decreasing maximum peak height of the pentacene Bragg reflections. The F6-TCNNQ and F4-TCNQ dopant molecules act as defects for the crystalline arrangement of the pentacene molecules under co-deposition conditions. The disturbance of this crystalline arrangement is stronger for doping with F6-TCNNQ, where the film is nearly amorphous for doping concentrations higher than 4 wt.%. For the F4-TCNQ doped pentacene, films are crystalline at least up to 8 wt.%. For both dopants, the polymorph II phase is destroyed at lower concentrations than the polymorph III phase. For the F6-TCNNQ doped pentacene films, no new Bragg reflections are detected compared to the undoped pentacene. On the contrary, at a F4-TCNQ doping ratio of 8 wt.% two new Bragg reflections appear besides the 001 reflection: the 110 and −101 reflection of the polymorph III phase (Fig. 1b). This means that a part of the molecules are oriented in two new directions and the preferred 001 orientation is strongly disturbed.

The determination of the crystallite size is done by the analysis of the shape of the Bragg reflections using the Scherrer equation and the Cauchy–Cauchy model as described in the experimental part. The microscopic strain in the film is disregarded for these calculations. The results are shown in Table 2. Due to the θ-2θ scan mode of the films, all determined crystallite sizes are those in perpendicular direction to the substrate surface. For the undoped pentacene film the crystallite size of the polymorph III crystallites is in the order of the overall film thickness of 150 nm, so the crystallites reach from the bottom to the top of the film. The crystallites of the polymorph II phase are in the range of 50 nm, which is smaller than the film

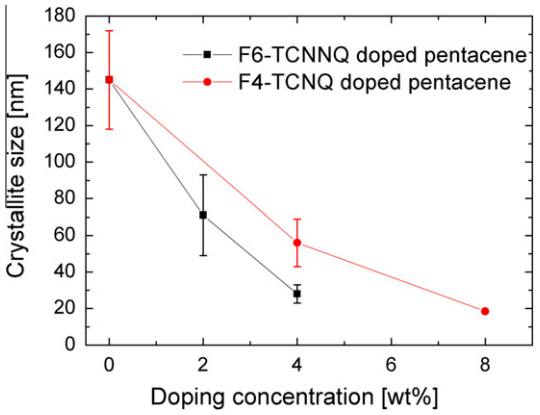

Fig. 3. Crystallite size of the polymorph III phase of pentacene in dependence of the molar doping concentration of F4-TCNQ and F6-TCNNQ doped pentacene films. Lines are drawn as guide to the eye.

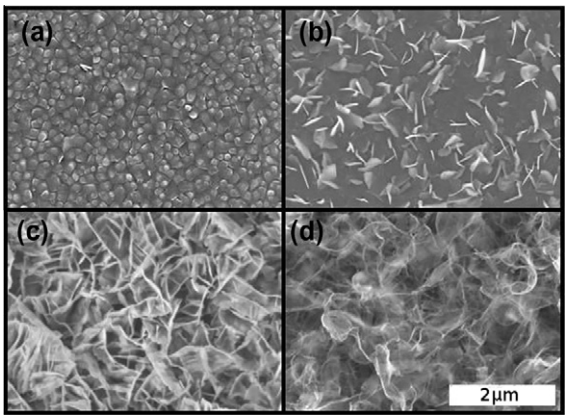

Fig. 4. Scanning electron micrograph of doped pentacene (the white scale bar in (d) is 2 μm). The images show a 150 nm thick film of pentacene grown on Si wafer with 50 nm of ALD Al_2O_3. Pure pentacene layer is labeled as (a). Doping concentrations of 2, 6 and 10 wt.% of F4-TCNQ are denoted as (b), (c) and (d), respectively. All films are prepared in the same manner as for the XRD measurements.

thickness. From the Bragg reflection height we can conclude that the larger number of the pentacene molecules are present in polymorph III phase.

F6-TCNNQ doping of pentacene drastically decreases the crystallite size as shown in Fig. 3 for the polymorph III crystallites. For 4 wt.% F6-TCNNQ doping, the crystallite size of the polymorph III phase is only 28 nm and no crystallites of the polymorph II exist anymore. For F4-TCNQ, the concentration has to be doubled (about 8 wt.%) to reduce film crystallites sizes down to the range of 18–28 nm, which means that the crystal structure of pentacene is more sensitive for F6-TCNNQ doping than for F4-TCNQ.

The arrangement of F4-TCNQ molecules deposited onto a crystalline film of pentacene monolayers has been investigated by Ha et al. [30]. They report that dopant molecules occupy vacancies within the pentacene crystal without disturbing the crystalline order. They conclude that due to size and molecular structure of F4-TCNQ molecules, diffusion of dopants into vacancies within the pentacene film is energetically favorable. Moreover, this arrangement enhances π-stacking between molecules. F6-TCNNQ molecules, however, are considerable larger than F4-TCNQ molecules. Presumably, this leads to different embedding conditions for F6-TCNNQ within the pentacene film. In contrast to [30], we study the formation of doped pentacene films under co-deposition conditions, which represents a very different situation for thin film growth. Nevertheless, in agreement to [30] we obtain for small doping concentrations of F4-TCNQ and F6-TCNNQ the formation of a crystalline phase. Thus, even it is reduced, but the tendency of formation of crystalline domains under co-deposition conditions is present. Additionally, we deduce from XRD investigations the appearance of an amorphous thin film phase. The fraction of this amorphous phase is strongly increasing upon doping. Differences between F6-TCNNQ and F4-TCNQ doped films likely arise because of the different molecule size.

XRD findings can be confirmed by analyzing SEM images of the recorded doped and undoped pentacene films. In Fig. 4 the strong change of the surface morphology in dependence of the doping concentration of F4-TCNQ is shown. The SEM micrograph of the undoped pentacene shows grains, whereas for the 2 wt.% F4-TCNQ doped pentacene film small plates pointing out of the sample surface between these grains. Starting from 4 wt.% doping concentration, the surface morphology completely changes to a sponge-like, very rough surface. Doping with F6-TCNNQ results in similar SEM images (not shown). Nevertheless, the XRD and SEM observations clearly show a loss of the crystalline structure of the film for larger doping. However, whether there is a tendency of dopant molecules to become embedded in the pentacene crystallites or to agglomerate in between them can not be concluded here. This is due to the fact that dopant agglomerations and pentacene crystallites can not be individually identified for doping concentrations larger than 6 wt.% in the SEM images for both dopants.

3.2. Field effect mobility

The dependence of the charge carrier mobility on the morphological changes in thin pentacene films induced by different evaporation conditions has been reported by Karl et al. [31]. They showed for doped pentacene films that a loss in field effect mobility can be related to a loss in structural order, which was concluded by analyzing the width of XRD rocking curves. In case of molecularly doped pentacene films, the observed dependency of charge carrier mobility measured in an OTFT configuration was considered to be caused by an increased impurity scattering [16].

Here, we can clearly correlate the XRD pattern of doped pentacene (Fig. 3) with the field effect mobility of the doped pentacene films (Fig. 5). Starting from undoped pentacene, we observe a continuous decay in mobility for increasing doping concentration. Apparently, this strong decay in mobility is related to the loss of crystalline order as shown in Fig. 3. The mobility is determined at $V_{GS} = -15$ V. This way we can ensure that I_{SD} is dominated by charge carriers injected from the source electrode and

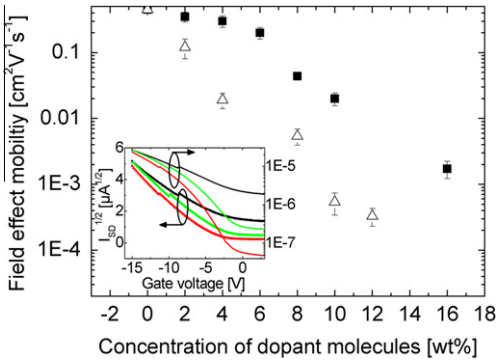

Fig. 5. Field effect mobility of pentacene OTFTs doped by F4-TCNQ (closed rectangles) and F6-TCNNQ (open triangles) for various doping concentrations. Mobility values are calculated by the slope of the gate voltage sweep at −15 V (saturation region). The inset shows a gate voltage sweep for different concentrations of dopant molecules of F4-TCNQ. The colors in the inset denote: 2 wt.% F4-TCNQ (red), 4 wt.% F4-TCNQ (green), 6 wt.% (black). The kink in graphs is an artifact due to the switch of the measurement range of the Keithley 2400 U. Error bars for mobility are taken from deviation of different devices built on the same sample. (For interpretation of the references to colour in this figure legend, the reader is referred to the web version of this article.)

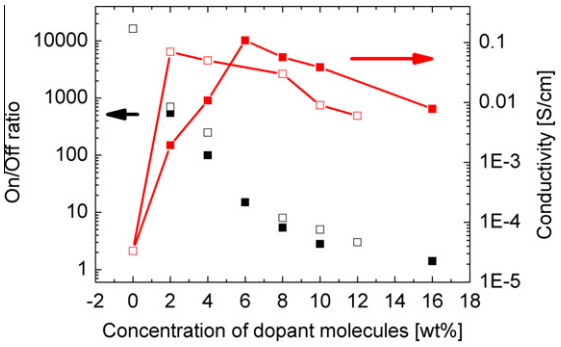

Fig. 6. On/off ratio (black) and the film conductivity (red) of the OTFTs consisting of pentacene doped by F4-TCNQ (closed rectangles) and F6-TCNNQ (open rectangles). Conductivity is measured in the OTFT geometry without applied gate voltage at a source-drain voltage of −10 V. Lines are drawn as guide to the eye. (For interpretation of the references to colour in this figure legend, the reader is referred to the web version of this article.)

not by charges provided by the dopant molecules. In general, the current in OTFTs of doped pentacene contains two contributions: a gate voltage independent bulk current and the current through the channel controlled by the gate. The evaluation of mobility at large V_{GS} by the slope of the transfer characteristics as done here has the advantage that this slope is not affected by the gate voltage independent off-state current originated from the bulk. As currently shown by Klauk and coworkers [32], molecular doping of DNTT employed in OTFTs leads to an increased off-state, but the OTFT performance measured in the saturation region is not strongly influenced.

The main motivation for doping is to improve the conductivity of the organic film, which is shown in Fig. 6. Up to 6 wt.% of F4-TCNQ mixed into the pentacene film, we obtain a superlinearly increasing conductivity, followed by an abrupt transition into a second regime characterized by a decrease of conductivity. In accordance with the XRD-patterns (see Fig. 2) and the mobility measurements (see Fig. 5), this transition occurs between 6 and 8 wt.% of dopant molecules. However, the improvement in conductivity is accompanied to a continuous decrease of the on/off ratio (defined as $I_{SD}(V_{GS} = -15\ V,\ V_{DS} = -15\ V)/I_{SD}(V_{GS} = 0\ V, V_{DS} = -15\ V)$ of the OTFTs. This conductivity is a bulk film conductivity, since the gate field modulation only occurs in the first few molecular layers of pentacene at the interface to the insulator.

For F6-TCNNQ doped pentacene films we obtain similar mobility and conductivity curves vs. doping concentration (see Fig. 5 and Fig. 6). Since the crystalline order of pentacene is more affected by F6-TCNNQ than by F4-TCNQ the maximum in conductivity is shifted to 2 wt.% of F6-TCNNQ. Moreover, mobility measurements provide a stronger decrease with increasing doping than for F4-TCNNQ doped samples.

To explain the two different slopes of the conductivity dependence we consider two mechanisms dominating the charge transport: transport in pentacene grains for polycrystalline structure and a hopping-like transport in the amorphous phase. We address this issue by discussing two important questions: Firstly, where are the dopant molecules located and secondly, what is the minimal crystallite size where the charge transport starts to be dominated by the hopping-like transport and not by the polycrystalline structure?

The first question was discussed by Maennig et al. [11]. They argued that the superlinear rise of the conductivity (see Fig. 6) can not be explained by an agglomeration of dopant molecules at grain boundaries. Thus, they concluded that dopant molecules must be embedded in the grains. Moreover they need to act as shallow acceptor states in order to explain the rise of conductivity [11]. These conclusions are in accordance to the finding of Ha et al. [30]. However, even if this is also very likely in our case, we can not conclude from XRD investigations whether dopant molecules are embedded in the grains or agglomerate in between them.

The second question is addressed in the literature in two different ways. On the one hand, percolations models [11] were used to describe transport via hopping between localized transport states. In this theory, the conductivity and the mobility depend on the overlap parameter. This parameter governs the tunneling rate from localized transport states. Thus, it is considered to be higher in ordered films and therefore, larger conductivity and mobility values are expected. The strong dependency of the overlap parameter on the structural order can explain the loss of conductivity and mobility observed here. This means that dopant molecules embedded in the pentacene crystallites give rise to an increasing conductivity for low doping concentrations due to an increased number of free charge carriers [7,15]. However, they can also cause a slightly decreasing mobility related to increased disorder. For larger doping concentrations, the complete loss of the crystalline order leads to a strongly reduced overlap parameter and therefore to reduced transport properties such as conductivity and mobility.

The second approach addressing the question of transport phenomena in such systems was discussed by

Horowitz et al. [33]. They distinguish between transport in grains and grain boundaries. Different grains are connected by grain boundaries states and thus the system can be treated as a back-to-back Schottky barrier. The conductivity and the mobility are described by the Matthiessen rule taking transport via grains and grain boundaries into account. Thus, for low doping concentrations the increasing conductivity can be explained by an increase of conductivity within the grains. The slightly decreasing mobility can be related to a stronger contribution of grain boundary states due to the reduced crystallite size. However, the assumption of the Schottky barrier formation remains valid until the Debye length is smaller than the crystallite size. The Debye length is given by

$$L_D = \sqrt{\frac{\varepsilon kT}{q^2 N}},$$

where ε is the dielectric constant of the material, k is the Boltzmann's constant, T is the temperature, q is the elementary charge, and N is the density of charges in the film (free charge carriers and charged dopant states). For a crystallite size smaller than the Debye length, the material can be treated as a uniform film. Thus, since doping gives rise to a strong decrease of the crystallite size, this model can explain the loss of mobility by complete loss of the crystalline phase. Despite this fact, the model fails for disordered films (or large doping concentrations), where the Debye length is larger than the crystallite size. Thus, this theory can not provide mobility values under such conditions.

However, both models discussed here can qualitatively explain the obtained dependencies of the mobility and the conductivity. The important parameters to describe the properties of charge transport are those describing the structural order. The structural order influences both the overlap of localized transport states and the relation between the crystallite size and the Debye length. Temperature dependent measurements on conductivity and mobility could provide a way to distinguish between the two charge migration models. For the percolation path model [11] an increased hopping probability for larger temperatures should lead to an increased conductivity and mobility. In contrast to that, for the transport mechanism via individual grains as proposed by Horowitz et al. [33] an increased Debye Length for increased temperature should not strongly affect the transport properties of the film for highly doped samples, where the crystallite size is already smaller than the Debye Length.

3.3. Vertical device structures

Doping of pentacene is not only interesting to reduce the contact resistance in OTFTs, it is also interesting for organic solar cells and vertical rectification diodes due to the improved conductivity and the control of important diode parameters. Thus, we are addressing the influence of the mobility of doped pentacene films for vertical diode-like devices. We study the mobility in vertical pentacene devices by space charged limited currents in order to show a general accordance between the horizontal field effect mobility and the mobility obtained in vertical dimension. However, the reader should be aware that different grain sizes and crystallographic orientations in horizontal and vertical direction do not allow for an exact comparison of the charge carrier mobility in both directions. The investigations on vertical device structures allow for a more reliable determination of mobility values at large doping concentrations in comparison to the OTFT measurements. This is due to the fact that in the OTFT geometry, the gate controlled source-drain current is superimposed by a strong bulk current contribution.

Vertical hole-only Schottky-diodes of pentacene are chosen to determine the hole mobility by analyzing space charge limited currents [3]. For these samples, the conductive polymer PEDOT:PSS acts as a buffer layer to improve the injection from the bottom electrode and to provide a smooth surface for the growth of pentacene films. Fig. 7 contains *IV* characteristics of devices at different doping ratios. As expected for space charge limited currents [34], we obtain for undoped pentacene a slope of two in the log–log scale of the *IV* curve at large voltages (>2 V), where all traps are filled. Thus, the mobility can be estimated by using Childs law

$$j = \frac{9}{8}\varepsilon\varepsilon_0\mu\frac{V^2}{d^3},$$

where j is the current density, V is the applied voltage, d is the thickness of the sample, ε_0 is the dielectric constant of the vacuum, and ε is the dielectric constant of pentacene. Here, we assume $\varepsilon = 3$. To guarantee the validity of Childs law, we prepared samples with different thicknesses of pentacene (not shown here). The thickness dependency of the current density in the SCLC regime obeys the required power law of $1/d^3$. For the sake of simplification, this SCLC model does not take into account effects of the electric field, the temperature, traps, and the charge carrier density on the charge carrier mobility. At low voltages, between 0.7 and 2 V traps dominate transport in pentacene. Filling of these traps at higher voltages allows computing of the mobility by employing Childs law. Thus, we obtain values for the mobility of 0.26 $cm^2 V^{-1} s^{-1}$ for undoped pentacene, 0.16 $cm^2 V^{-1} s^{-1}$ for pentacene doped with 4 wt.% F4-TCNQ and 0.09 $cm^2 V^{-1} s^{-1}$ for pentacene doped with 6 wt.% F4-TCNQ, which is in accordance to values estimated from

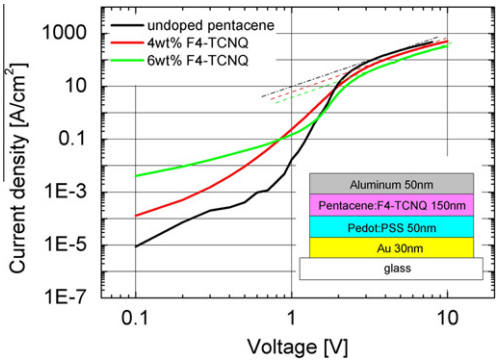

Fig. 7. Current voltage characteristics of pentacene Schottky-diodes in forward direction. The dotted lines are drawn to illustrate the Childs law. The device structure is shown as inset.

the OTFT measurements (0.45 $cm^2V^{-1}s^{-1}$ for undoped, of 0.3 $cm^2V^{-1}s^{-1}$ for 4 wt.% F4-TCNQ, 0.2 $cm^2V^{-1}s^{-1}$ for 6 wt.% of F4-TCNQ).

However, even if the trap free SCLC region for voltages >2 V provides reasonable values for the mobility, the effect of dopant molecules on the distribution and the occupancy of traps has to be considered. The contribution of traps states can be seen in the low voltage region (<0.7 V) in Fig. 7. The pure pentacene film exhibits an intrinsic trap density causing a trap limited current. Dopant molecules can be treated as shallow acceptors states since they provide free charges at room temperature. This leads to an increase of conductivity at low voltages (see also Fig. 5). An increase and a broadening of the total density of states by adding dopant molecules to pentacene has been discussed elsewhere [7,15]. The increase of the current in the low voltage region with increasing doping concentration up to 6 wt.% can be explained by a filling of native trap states of the pentacene by charge carriers provided by the dopants. Hence, doping gives rise to an increased conductivity but it also causes the reduced mobility by decreasing crystallite size. Related to the stronger influence of F6-TCNNQ on the film morphology, no clear SCLC behavior is observed even for low dopant concentrations of 2 wt.%.

Nevertheless, the values of mobility provided by SCLC measurements for the doping by F4-TCNQ confirm the trend obtained by OTFT investigations. The analysis by SCLC remains valid for low doping concentrations, where the polycrystalline phase within the film dominates the charge transport properties. For larger doping concentrations, we do not obtain *IV* characteristics describable by the SCLC model indicating a change in the dominant charge transport regime.

Thus, the loss of mobility can clearly be related to a doping-induced structural phase transition in the film. Whether this structural phase transition additionally gives rise to a change in the trap distribution of pentacene can not be concluded here. This could probably be studied by deep level transient spectroscopy (DLTS).

4. Summary

In conclusion, we studied molecular doping of pentacene by F4-TCNQ and F6-TCNNQ and its effect on structural properties and the charge carrier mobility. We reveal the appearance of a crystalline and an amorphous thin film phase induced by doping under co-deposition conditions. The fraction of the amorphous phase within the film is increased for larger doping concentrations. A strong drop of crystallite size is obtained at a doping concentration of around 7 and 4 wt.%, respectively. The difference between the dopants likely arises because of their difference in size and their tendency to be embedded within a crystalline structure. Moreover, we investigated the influence of this structural change on the charge carrier mobility. The hole mobility shows a discontinuous drop of more than 2 orders of magnitude in the OTFT geometry for pentacene films doped by F4-TCNQ. In particular, the mobility has a weak dependence on the doping concentration below 6 wt.% for F4-TCNQ. Beyond 6 wt.% we obtain a strong drop of the mobility. This behavior can be explained by a continuously decreasing crystallite size of doped pentacene leading to an entire amorphous phase for large doping concentrations. From SCLC measurements we conclude that small concentrations (<7 wt.% for F4-TCNQ) of molecular dopants in pentacene lead to a filling of native trap states in pentacene and a slightly decreasing mobility due to a decreasing crystallite size. For larger doping concentrations (>7 wt.% for F4-TCNQ) the transport is not dominated by the polycrystalline structure of pentacene. It is governed by hopping-like transport between localized transport states in an amorphous film.

We believe that these results are not only interesting from perspective of the material properties of organic crystalline film. They are also of general interest for applications since pentacene is a material used for organic thin film transistors, organic solar cells and high-frequency diodes, where the control of conductivity by doping is a basic requirement.

Acknowledgements

This project has been funded by the Bundesministerium für Bildung und Forschung (BMBF) within the project 13N9872 and the Alexander von Humboldt Foundation.

References

[1] S. Reineke, F. Lindner, G. Schwartz, N. Seidler, K. Walzer, B. Lüssem, K. Leo, Nature 459 (2009) 234–238.
[2] C.W. Tang, Appl. Phys. Lett. 48 (1986) 183.
[3] S. Steudel, K. Myny, C. Deibel, S. de Vusser, J. Genoe, P. Heremans, Nat. Mat. 4 (2005) 597.
[4] G. Horowitz, Adv. Mat. 10 (1998) 365–377.
[5] H. Kleemann, R. Guitierrez, F. Lindner, S. Avdoshenko, P.D. Manrique, B. Lüssem, G. Cuniberti, K. Leo, Nano Lett. 10 (2010) 4929–4934.
[6] V.I. Arkhipov, P. Heremans, E.V. Emelianova, H. Bässler, Phys. Rev. B 71 (2005) 045214.
[7] K. Walzer, B. Maennig, M. Pfeiffer, K. Leo, Chem. Rev. 107 (2007) 1233–1271.
[8] R.S. Nohr, P.M. Kuznesof, K.J. Wynne, M.E. Kenney, P.G. Siebenman, J. Am. Chem. Soc. 10 (1981) 4371–4377.
[9] M.F. Calhoun, J. Sanchez, D. Olaya, M.E. Gershenson, V. Podzorov, Nat. Mat. 7 (2008) 84–89.
[10] G. Parthasarathy, C. Shen, A. Kahn, S.R. Forrest, Appl. Phys. 89 (2001) 4986.
[11] B. Maennig, M. Pfeiffer, A. Nollau, X. Zhou, K. Leo, P. Simon, Phys. Rev. B 64 (2001) 195208.
[12] D. Ray, K.L. Narasimhan, J. Appl. Phys. 108 (2008) 093711.
[13] S. Olthof, W. Tress, R. Meerheim, B. Lüssem, K. Leo, J. Appl. Phys. 106 (2009) 103711.
[14] O. Tal, Y. Rosenwaks, Y. Preezant, N. Tessler, C.K. Chan, A. Kahn, Phys. Rev. Lett. 95 (2005) 256405.
[15] C. Vanoni, T.A. Jung, S. Tsujino, Appl. Phys. Lett. 94 (2009) 253306.
[16] K. Harada, M. Sumino, C. Adachi, S. Tanaka, K. Miyazaki, Appl. Phys. Lett. 96 (2010) 253304.
[17] M. Brinkmann, V.S. Videva, A. Bieber, J.J. Andre, P. Turek, L. Zuppiroli, P. Bugnon, M. Schaer, F. Nuesch, R. Humphry-Baker, J. Phys. Chem. A 108 (2004) 8170–8179.
[18] D. Knipp, R.A. Street, A. Völkel, J. Ho, J. Appl. Phys. 93 (2003) 347–355.
[19] S. Yoo, B. Domercq, B. Kippelen, Appl. Phys. Lett. 85 (2004) 5427–5429.
[20] K. Harada, A.G. Werner, M. Pfeiffer, C.J. Bloom, C.M. Elliott, K. Leo, Phys. Rev. Lett. 94 (2005) 036601.
[21] W. Kraus, G. Nolze, J. Appl. Cryst. 29 (1996) 301–303.
[22] PowderCell 2.3, Bundesanstalt für Materialforschung und –prüfung (BAM), Berlin, 1999.
[23] Program ANALYZE, Rayflex Version 2.285, Rich. Seifert & Co., 2000.
[24] A.A. Levin, SIZECR program, Institut für Strukturphysik, Technische Universität Dresden, Dresden, 2007.
[25] X. Pang, K. Gao, F. Luo, Y. Emirov, A.A. Levin, A.A. Volinsky, Thin Solid Films 517 (2009) 1924.

[26] C. Schuenemann, C. Elschner, A.A. Levin, M. Levichkova, K. Leo, M. Riede, Thin Solid Films 519 (2011) 3939–3945.
[27] P.G. Taylor, J.-K. Lee, Al.A. Zakhidov, M. Chatzichristidi, H.H. Fong, J.A. DeFranco, G.G. Malliaras, C.K. Ober, Adv. Mat. 21 (2009) 2314.
[28] S. Schiefer, M. Huth, A. Dobrinevski, B. Nickel, J. Am. Chem. Soc. 129 (2007) 10316.
[29] T. Siegrist, C. Besnard, S. Haas, M. Schiltz, P. Pattison, D. Chernyshov, B. Batlogg, C. Kloc, Adv. Mater. 19 (2007) 2079.
[30] S.D. Ha, A. Kahn, Phys. Rev. B. 80 (2009) 195410.
[31] N. Karl, Syn. Met. 133-134 (2003) 649–657.
[32] F. Ante, D. Kälblein, U. Zschieschang, T.W. Canzler, A. Werner, K. Takimiya, M. Ikeda, T. Sekitani, T. Someya, H. Klauk, Small 7 (2011) 1186–1191.
[33] G. Horowitz, M.E. Hajlaoui, R. Hajlaoui, J. Appl. Phys. 87 (2000) 4456–4463.
[34] S. Nebpurer, E.A. Silinsh, Phys. Stat. Sol. A 34 (1976) 747.